Electronic structure and thermopower of $Ni(Ti_{0.5}Hf_{0.5})Sn$ and related half-Heusler phases

L. Chaput,[1] J. Tobola,[2] P. Pécheur,[1] and H. Scherrer[1]
[1]*Laboratoire de Physique des Matériaux, UMR 75560, ENSMN, Parc de Saurupt, 54042 Nancy, France*
[2]*Faculty of Physics and Applied Computer Science, AGH University of Science and Technology, Al. Mickiewicza 30, 30-059 Cracow, Poland*

(Received 9 September 2005; revised manuscript received 13 December 2005; published 25 January 2006)

In this paper we investigate the electronic structure and the thermopower for $Ni(Ti_{0.5}Hf_{0.5})Sn$ and related half-Heusler compounds. Two different methods have been used to calculate the electronic structure, i.e., full potential linearized augmented plane wave method for ordered compounds and the Korringa-Kohn-Rostoker method within the coherent potential approximation for disordered alloys. We show that these methods give very close results if comparing the density of states obtained in both cases. Moreover, no peculiarities in the band structure have been revealed upon alloying the parent compounds and therefore the large value of the thermopower reported experimentally for $Ni(Ti_{0.5}Hf_{0.5})Sn$ with respect to NiTiSn or NiHfSn, does not have an origin in the electronic structure behavior. The thermopower calculations performed for different half-Heusler compounds rather suggest that the carrier concentration itself could be predominantly responsible for the large thermopower in $Ni(Ti_{0.5}Hf_{0.5})Sn$ as well as in other half-Heusler phases. Therefore, the large negative values of the Seebeck coefficient are not limited to some specified half-Heusler semiconductors but seem to be the rule for the *n*-type samples with moderately low carrier concentrations.

DOI: 10.1103/PhysRevB.73.045121 PACS number(s): 71.15.Mb, 72.10.Bg, 72.20.Pa

I. INTRODUCTION

Half-Heusler phases are well-known compounds studied for their wide variety of physical properties including magnetism,[1] half-metallic ferromagnetism,[2] and shape memory effect.[3] Due to the fact that many 18-valence electron half-Heusler systems are narrow band gap semiconductors (see e.g.[4,5]), they were also examined for the generation of thermoelectricity.[6,7] In order to get the best efficiency of the thermoelectric material one should maximize the figure of merit $ZT=S^2\sigma T/\kappa$, where S, σ, and κ represent thermopower, electrical, and thermal conductivity, respectively. Unfortunately, the half-Heusler systems were established to have quite important thermal conductivity κ and not sufficiently large thermopower S to compete with the "state of art" thermoelectric materials.[8] Interestingly, a very large thermopower (about $-300\ \mu V/K$) has been reported[9,10] in half-Heusler alloys with the general formula Ni(Ti,Zr,Hf)Sn, containing Hf and/or Zr atoms substituted on Ti-site. This large S value is much greater than the thermopower values currently measured for NiTiSn and NiHfSn parent compounds (about $-150\ \mu V/K$, see, e.g., Ref. 9). An understanding of these phenomena could be of great interest from the application point of view, since the thermopower appears squared in the figure of merit. Note, that substitution with isoelectronic elements can also be beneficial for the thermal conductivity due to the atomic mass defects (without substantial modifications of electronic properties).

Hence, the goal of this paper was to search for the origin of the thermopower enhancement in the disordered half-Heusler materials.

At first sight, such behavior could arise from some peculiarities in the electronic structure because of the quite different nature of *d* orbital for Ti and Hf, which are known to play a decisive role in the binding of these compounds (see Sec. II and Refs. 11 and 12). However, as will be shown in Sec. II, this is not the case in $NiTi_{0.5}Hf_{0.5}Sn$. In Sec. III the calculated thermopower will be presented, as a function of carrier concentration, for NiTiSn, NiZrSn, NiHfSn, $NiTi_{0.5}Hf_{0.5}Sn$, being in good agreement with available experimental data. Then, this supports the suggestions that the large values of Seebeck coefficients might be the rule for half-Heusler systems with low carrier concentration and with a microstructural state with as few secondary phases as possible. We believe that these indications should have some importance for the optimization of the thermoelectric properties in half-Heusler compounds.

II. ELECTRONIC STRUCTURE FOR $NiTi_{0.5}Hf_{0.5}Sn$

A large thermopower has been reported for NiTiSn-based half-Heusler alloys, if the Ti atoms are partly replaced with Hf or both with Hf and Zr atoms. We call these alloys with the general formula Ni(Ti,Zr,Hf)Sn.

The electronic structure of $NiTi_{0.5}Hf_{0.5}Sn$ has been investigated in details and taken as a model case, since within all Ni(Ti,Zr,Hf)Sn samples this composition was expected to exhibit the largest differences with respect to the well-known NiTiSn and NiHfSn compounds. Since the thermopower has been found much smaller (about $-150\ \mu V/K$) for the endpoint compounds[9] some electronic structure peculiarities might give rise to a strong increase of thermopower. Once the chemical composition has been specified our model system is not fully defined. In fact, the analysis performed in Ref. 9 does not reveal its crystal structure. We can therefore consider two extreme descriptions for this system: a fully ordered (FO) compound where exactly two of four Ti atoms per unit cell are substituted by Hf atoms, but also a fully disordered (FD) alloy, where Hf atoms are distributed randomly on the Ti sites with two Hf atoms per unit cell only on average. The electronic structure of $NiTi_{0.5}Hf_{0.5}Sn$ has then been calculated in both cases.

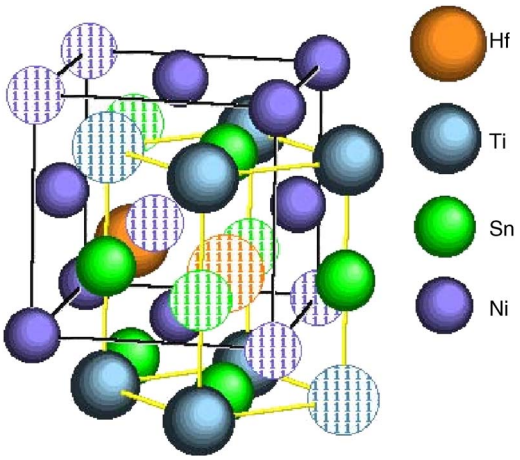

FIG. 1. (Color online) Cubic (black) and tetragonal (yellow) cell for the half-Heusler system. The dashed atoms belong to the planes (101) and (112); see text.

A. Fully ordered (FO) compound

A unit cell of the FO compound is shown in Fig. 1. While perfectly ordered half-Heusler compounds NiTiSn and NiHfSn have cubic symmetry with space group $F\bar{4}3m$ (black cell in Fig. 1), our FO model system is tetragonal and belongs to the space group $P\bar{4}m2$ (shown with a yellow cell in Fig. 1).

The electronic structure of this compound was calculated using the full potential linearized augmented plane wave (FLAPW) WIEN2k program.[13] The self-consistency cycle was achieved with 1000 k points in the Brillouin zone. The exchange-correlation potential was computed in the generalized gradient approximation (GGA) approach using the Perdew-Burke-Erzenhof functional.[14] The unit cell has been optimized employing the relation $c=\sqrt{2}a$. In our notation c is the lattice parameter of the cubic cell or equivalently the c axis for the tetragonal cell, and a is the lattice parameter in the basal plane of that cell. At equilibrium we found $c=11.452$ a.u.; the value can be compared to those for NiTiSn and NiHfSn. The computed lattice parameters are then reported in Table I together with those previously calculated[12] and the experimental data.

A good agreement was found, since for NiTiSn and NiHfSn our results are of order of 1% larger than the experimental values. The small differences with Ref. 12 might be attributed to a different choice of *muffin-tin* radius

TABLE I. Lattice parameter and band gap E_g for NiTiSn, NiHfSn and $NiTi_{0.5}Hf_{0.5}Sn$.

	c(a.u.) present calculation	c(a.u.) Ref. 12	c(a.u.) experiments[a]	E_g (eV)
NiTiSn	11.271	11.261	11.187	0.45
NiHfSn	11.589	11.572	11.463	0.39
$NiTi_{0.5}Hf_{0.5}Sn$	11.452	-	-	0.46

[a]Refs. 11 and 12.

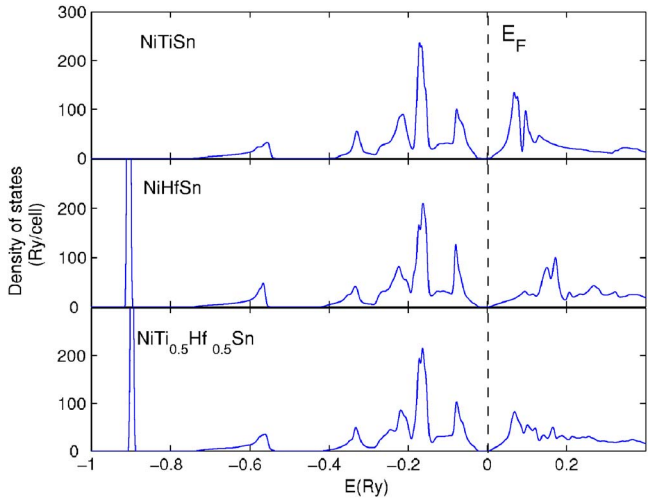

FIG. 2. (Color online) Density of states for NiTiSn, NiHfSn, and FO $NiTi_{0.5}Hf_{0.5}Sn$.

($R_{mt}=2.2$ a.u. in all present calculations) since the other parameters were taken to be the same. We see also that $NiTi_{0.5}Hf_{0.5}Sn$ almost obeys Vegard's law indicating a continuous change through the substitution of Ti by Hf.

In Fig. 2 and Fig. 3 we show density of states (DOS) and energy bands $E(\mathbf{k})$ for NiTiSn, NiHfSn, and FO $NiTi_{0.5}Hf_{0.5}Sn$. A detailed explanation of the electronic structure in NiTiSn can also be found in Refs. 11, 12, and 15. At first sight, DOSs for all three compounds look quite similar. The s states of Sn are located about 0.6 Ry below E_F. At the Fermi level we found a gap opened by hybridization between d states of Ni and Ti or Hf. The d states below E_F comes essentially from Ni d orbitals, whereas those above E_F are mainly due to Ti d or Hf d orbitals. The only important difference between these compounds (Fig. 2) comes from the location of d-like states with respect to E_F. In NiTiSn and $NiTi_{0.5}Hf_{0.5}Sn$ Ti-d and Hf-d states are located about 0.09 Ry above the gap, whereas Hf-d states go up to 0.15 Ry in NiHfSn. This presumably results in a smaller energy gap for NiHfSn (see Table I). Such behavior can be explained from the fact that orbitals are much more localized for Hf than for Ti. To support our suggestion, the maps of electron densities have been plotted (Fig. 4) along planes going through the same crystallographic position both in cubic (along 101 plane) and tetragonal (along 112 plane) structures. The hybridization is therefore stronger between Ni and Ti than between Ni and Hf in both cases. Consequently, this leads to the band gap shrinking in NiHfSn, since the states near the conduction band edge are still of Ni-d character.

Looking at the band structure for FO $NiTi_{0.5}Hf_{0.5}Sn$, as illustrated in Fig. 3, it may be surprising that a direct gap at Γ point appears, unlike the well-established indirect gap in the cubic NiTiSn and NiHfSn (Fig. 3). This comes simply from the folding of bands when going from cubic to tetragonal cell, since the ΓX vector of the cubic cell belongs to the reciprocal lattice of the tetragonal cell.

B. Fully disordered (FD) compound

In the next section the results of the thermopower calculations will be presented for NiTiSn, NiHfSn, and

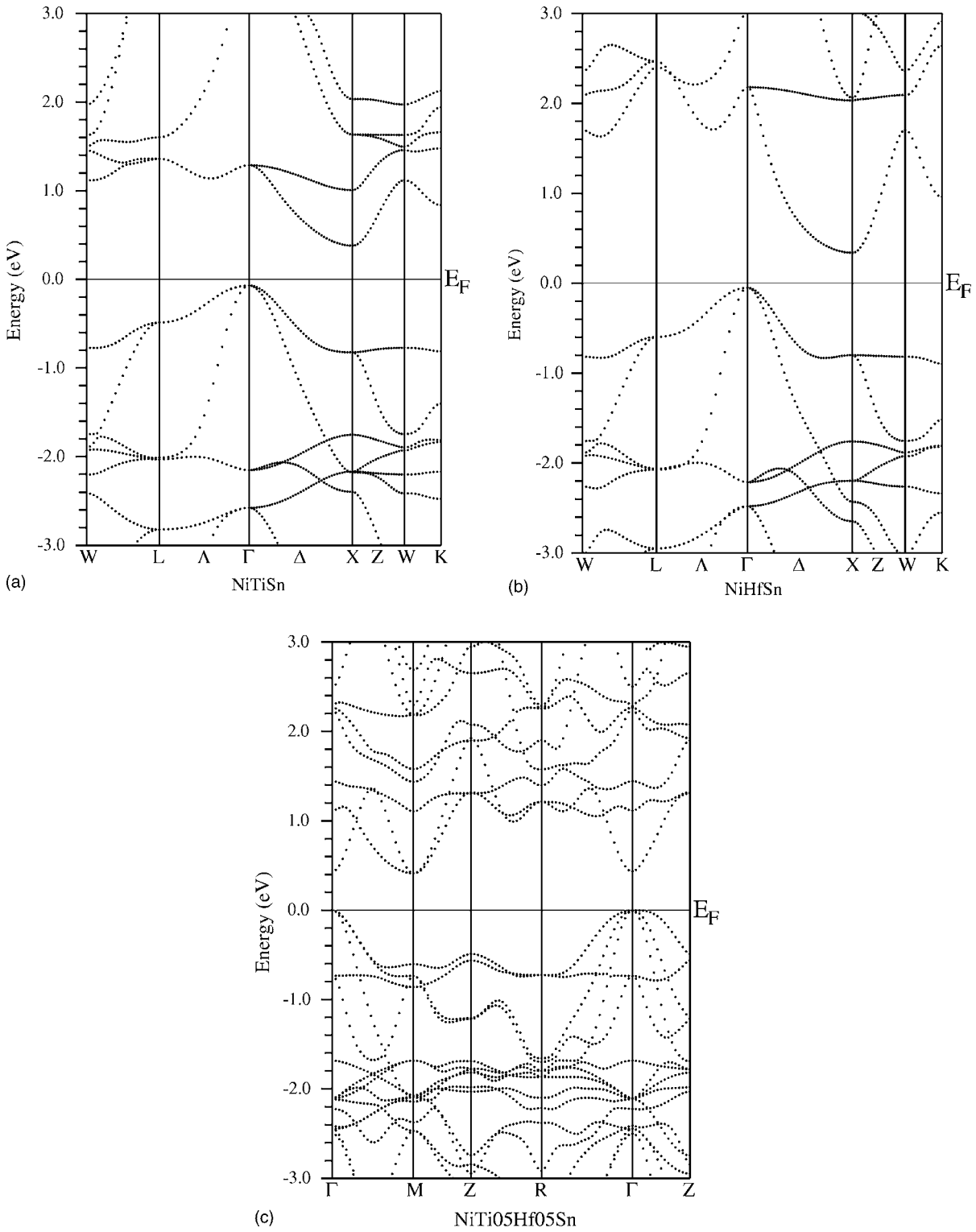

FIG. 3. Energy bands for NiTiSn, NiHfSn, and FO $NiTi_{0.5}Hf_{0.5}Sn$.

$NiTi_{0.5}Hf_{0.5}Sn$ using the electronic structure obtained for perfectly ordered compounds. In order to verify if such electronic structure approximation is satisfying for Ni(Ti,Hf)Sn alloys, we have also performed electronic structure calculations assuming that the compounds are fully disordered. The charge self-consistent Korringa-Kohn-Rostoker (KKR) method within the coherent potential approximation (CPA) has been then applied to compute density of states in the half-Heusler $NiTi_{1-x}Hf_xSn$ with $x=0.0$, 0.25, 0.50, 0.75, and 1. The KKR-CPA calculations have been done in the same way as for other half-Heusler phases[16] (more details about the KKR-CPA methodology can be found in Refs. 17 and 18). The obtained DOS are quite close to those shown in Fig. 2 and therefore they have not been reproduced. However, in

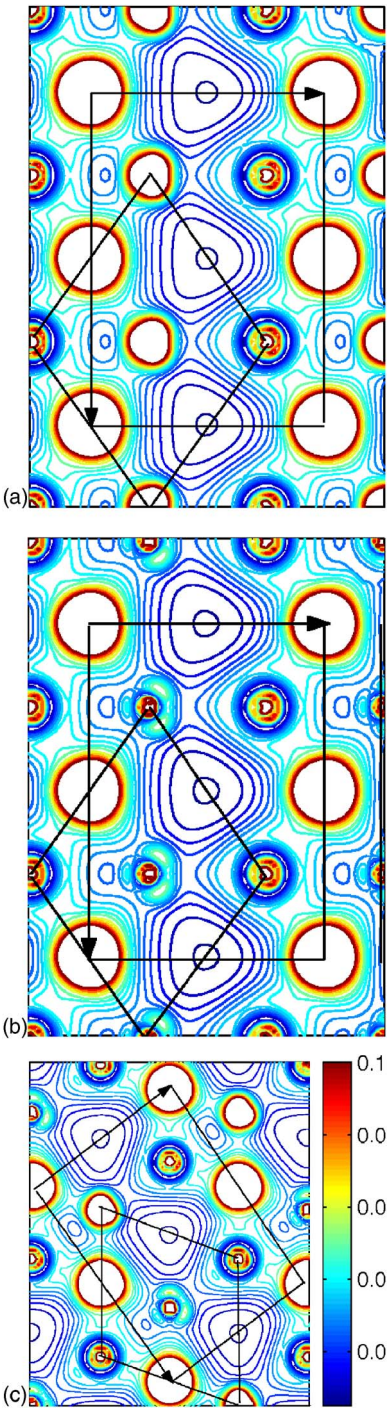

FIG. 4. (Color online) Isodensity plot for NiTiSn, NiHfSn, and FO $NiTi_{0.5}Hf_{0.5}Sn$. The unit is e/a.u.[3]

Fig. 5 we zoom on the energy window near the conduction band that is relevant to the electron concentrations which are taken into account in the thermopower calculations (next section). We see from the KKR-CPA results that the DOS slope (Fig. 5) increases more or less continuously when the concentration of Ti atoms increases from 0 to 1. This characterizes well a virtual crystal behavior. A similar tendency is observed in the periodic FLAPW calculations (Fig. 6).

So in our cases, similarities between FLAPW and KKR-CPA results would indicate that the electronic properties of

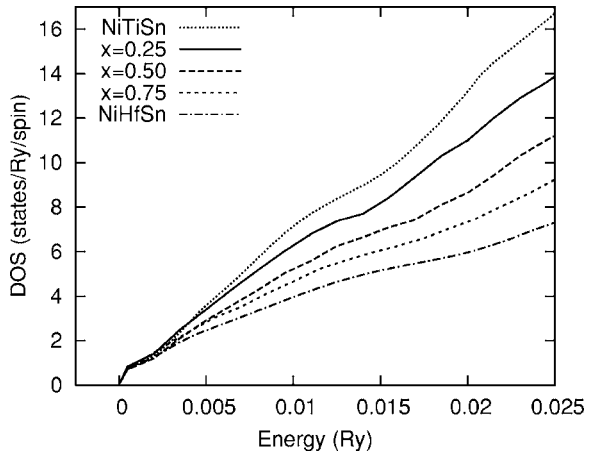

FIG. 5. KKR-CPA density of states calculated in FD $NiTi_{1-x}Hf_xSn$.

investigated materials are only weakly sensitive to the particular choice of the crystal structure description. This allowed us selecting the most convenient structure to calculate the transport coefficients.

III. THERMOPOWER

In the previous section we have seen that the larger thermopower observed in $NiTi_{0.5}Hf_{0.5}Sn$ does not originate from electronic structure anomalies with respect to the end-point compounds. This is also supported by direct calculations of the thermopower.

Looking at experimental data of electron transport properties reported for different half-Heusler semiconducting phases, we can notice a remarkable diversity of the measured thermopower values (even for nominally the same material, see Table II). As suggested by Uher *et al.* in Ref. 6, the measured thermopower significantly depends on the way the samples have been obtained. For example, as the annealing time increases, the amount of the secondary phases (presum-

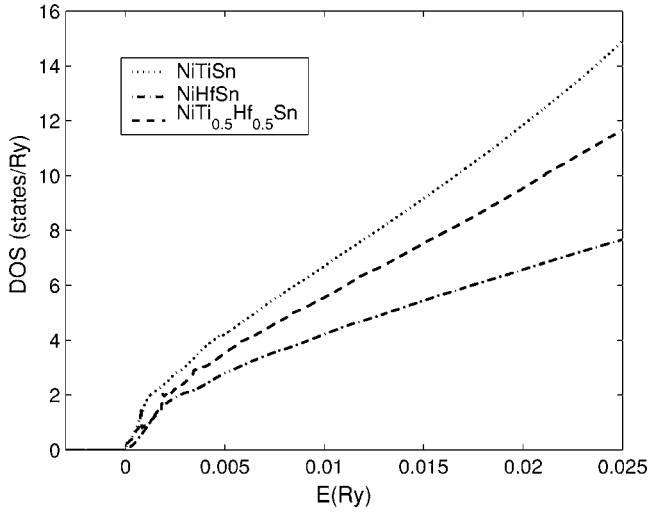

FIG. 6. FLAPW density of states for NiTiSn, NiHfSn and FO $NiTi_{0.5}Hf_{0.5}Sn$ (the same energy range of energy as in Fig. 5

TABLE II. Experimental (at room temperature) thermopower and carrier concentration for investigated half-Heusler alloys. n_H is specified per cell of $Ni_2A_2Sn_2$, where A=Ti, Zr, or Hf.

	S (μV/K)	n_H	Ref.
NiTiSn	−142		9
NiTiSn	−270	0.000 83	19
NiTiSn	−318		20
NiZrSn	−167	0.021	6
NiZrSn	−171	0.0103	6
NiZrSn	−210	0.0024	6
NiZrSn	−176		9
NiZrSn	−520	$4.7\ 10^{-5}$	21
NiHfSn	−124		9
$NiTi_{0.5}Hf_{0.5}Sn$	−281		9
$NiTi_{0.5}Hf_{0.5}Sn$	−250		20
$NiTi_{0.5}(Zr_{0.5}Hf_{0.5})_{0.5}Sn$	−325		10

ably metallic) decreases, leading to a larger thermopower. One may expect that the experimental conditions could also be the reason for the large difference between the thermopower of NiTiSn and $NiTi_{0.5}Hf_{0.5}Sn$. But the question is if we should attribute these differences to an averaging of the thermopower between two different ordered phases, or to a drastic change in the scattering mechanism, or simply to the number of conducting electrons? In real systems, these phenomena are certainly connected, but it would be useful to know which aspect is the most significant for future thermopower optimization in this family of compounds.

To this end, the thermopower has been calculated for NiTiSn, $NiTi_{0.5}Hf_{0.5}Sn$, and NiHfSn. The isoelectronic NiZrSn compound has also been considered, since a number of experimental data exist in the literature. The experimental results are shown in Fig. 7 for the cases where both thermopower and electron carrier concentration data from Hall measurements (see Table II) are available. For other cases only the thermopower values have been reported.

The thermopower was evaluated at room temperature using the computational method recently applied to calculate electron transport coefficients in $CoSb_3$ based skutterudites.[22] Since the theoretical background has been presented there,[22] we only briefly comment how the thermopower is derived. First, the electronic structure obtained in Sec. II A was used to calculate the transport function

$$\bar{\bar{\sigma}}(E) = \frac{q^2}{V}\sum_{kn} \tau_{kn}\vec{v}_{kn}\vec{v}_{kn}\delta(E - E_{kn}), \tag{1}$$

which is the central quantity in the electron transport calculations. In fact, this function contains all needed information for the investigated system as electron velocities $\vec{v}_{kn}$, relaxation times τ_{kn}, and energy levels E_{kn}.

Next, the Onsager coefficients L_{ij}, defining main transport coefficients as electrical conductivity σ, thermopower S, Hall concentration n_H, and Lorenz factor L, are obtained from the following expression:

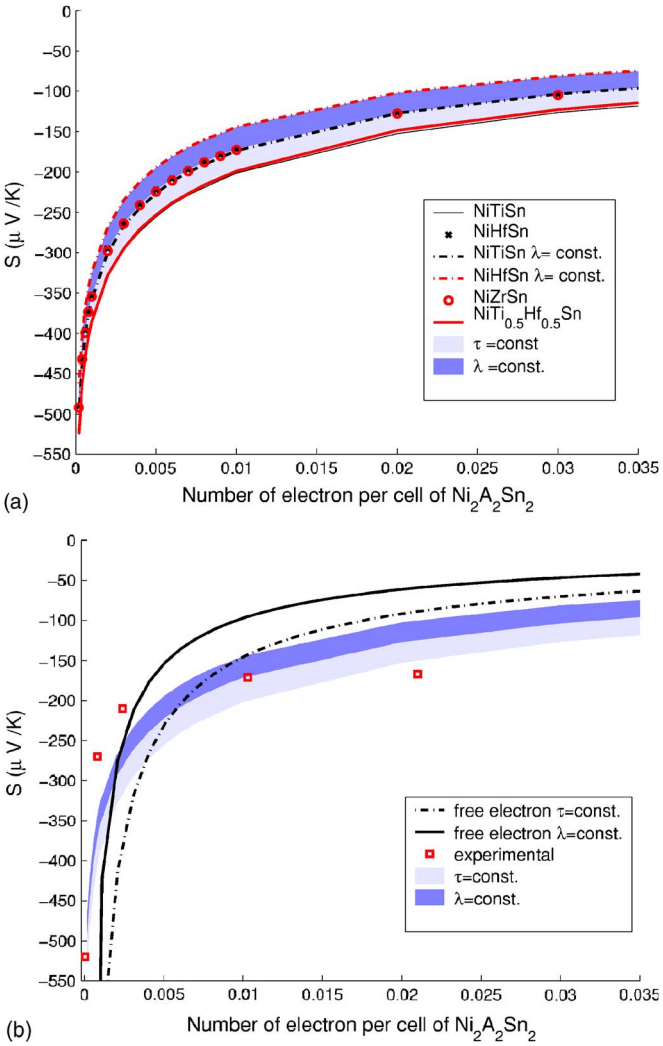

FIG. 7. (Color online) Calculated and experimental thermopower at room temperature. When not specified the relaxation is considered as constant. The dependence of the thermopower with the electron concentration is obtained by varying the chemical potential in Eq. (1) and using $n = \int^{\mu} d\varepsilon f_0(\varepsilon) g(\varepsilon)$. Note that in the upper panel the NiZrSn and NiTiSn (λ=const) curves respectively represented as red dotted and black dashed-dotted line are very close.

$$L_{ij} = \int dE \left(\frac{E-\mu}{q}\right)^{i+j-2} \frac{\partial f_0}{\partial \mu} \bar{\bar{\sigma}}(E), \tag{2}$$

where the chemical potential μ derivation of the Fermi-Dirac function f_0 also appears. In particular, the thermopower is calculated from the well-known relation

$$S = \frac{1}{T} L_{11}^{-1} L_{12} \tag{3}$$

$$= \frac{1}{T}\left(\int d\varepsilon \bar{\bar{\sigma}}(\varepsilon)\frac{\partial f_0}{\partial \mu}\right)^{-1}\left(\int d\varepsilon \frac{1}{q}\bar{\bar{\sigma}}(\varepsilon)(\varepsilon-\mu)\frac{\partial f_0}{\partial \mu}\right). \tag{4}$$

The most important steps of the applied procedure are sketched in Fig. 8 but more explanations are given in Ref. 22.

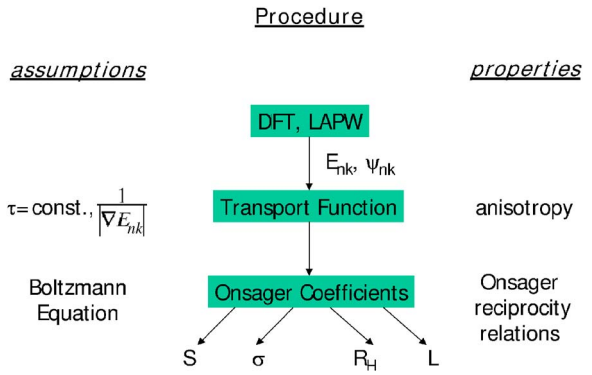

FIG. 8. (Color online) The general scheme of the electron transport coefficients calculations. Note that only thermopower is analyzed in the present work.

Two particular cases have accounted for the present thermopower calculations:

(i) The constant relaxation time approximation (τ=const); in this case the thermopower S becomes independent on τ since the relaxation time cancels in Eq. (4).

(ii) The constant mean free path approximation ($\lambda=\tau_k v_k$=const), which is in fact equivalent to the impurity scattering approach.

The corresponding thermopower results obtained in the entitled half-Heusler systems are collected in Fig. 7. The dark blue (gray) area presents the results obtained within λ=const, where the upper limit corresponds to NiHfSn and the lower one to NiTiSn. The light blue (gray) area illustrates the results gained within τ=const, where (as in the previous case) the upper limit corresponds to NiHfSn and the lower one to NiTiSn. Noteworthy, the results for NiZrSn and NiTiSn (λ=const) are nearly identical. In Fig. 7 the thermopower curve corresponding to $NiTi_{0.5}Hf_{0.5}Sn$ is also shown and is found slightly above the NiTiSn curve. In both approximations the curves computed for $NiTi_{0.5}Hf_{0.5}Sn$ and NiZrSn belong to the area bordered upward by the NiHfSn curve and downward by the curve for NiTiSn. In this case the thermopower behaviors agree with expectations from the simple considerations: Ti d states are located closer E_F than the Hf d states, the slope of the density of states in the vicinity of E_F is smaller in the case of Hf than for Ti (see Fig. 5) and therefore the thermopower follows more or less the DOS modifications. Moreover, the concentration dependent Seebeck coefficient variations are very close for NiZrSn and NiHfSn. An important observation (in Fig. 7) is that the experimental thermopower changes strongly with the carrier concentration n. These variations are well reproduced by the calculations and much better than fitted with the free electron curves. This shows that the carrier concentration n should be regarded as an important factor when optimizing the thermopower of half-Heusler alloys, since the $S(n)$ variation alone is sufficient to reproduce quite well the experimental value of S, when both thermopower and carrier concentration data are available. One can also conclude from Fig. 7 that the details of the scattering mechanism are less important than the carrier concentration. However, as expected, these curves suggest that we start from a λ=const regime as the carrier concentration increases.

These results can also be helpful to understand the unconventionally large values reported for the thermopower of Ni(Ti,Hf)Sn and Ni(Ti,Zr,Hf)Sn alloys in Refs. 9 and 10. In fact, our calculations suggest that the electron carrier concentration could be at the origin of these large values (see Table II) as it is the case for NiTiSn compounds produced in Ref. 19. Even if there is no direct proof of this conclusion for all Ni(Ti,Zr,Hf)Sn alloys, since the electron concentration has not been measured there, we do hope that the theoretical results will motivate further experimental investigations. Strictly speaking, the above-mentioned discussion can only be applied to Ni(Ti,Hf)Sn alloys since this case was considered in the calculations. In Ni(Ti,Zr,Hf)Sn alloys, Zr atoms could give additional effects. However, we have shown that $NiTi_xHf_{1-x}Sn$ follows a virtual crystal behavior, mainly due to the fact that Ti and Hf are isoelectronic. Since Zr is also isoelectronic to these atoms, a virtual crystal behavior is also expected for Ni(Ti,Zr,Hf)Sn alloys. The discussion above should therefore also be valid but there is still no carrier concentration measurement available in this case.

IV. CONCLUSIONS

We have shown using different electronic structure calculations (FLAPW and KKR-CPA), applied to extreme crystallographic approximations (FO and FD), that there is no unusual behavior of electronic structure in Ni(Ti,Hf)Sn alloys that could explain the marked enhancement of thermopower[9,10] with respect to NiTiSn and NiHfSn.

On the other hand, the thermopower calculations within two different approximations for electron scattering (τ=const and λ=const) have evidenced that the electron carrier concentration n can give itself such a large negative thermopower for the lowest carrier concentration. This might be an explanation for the large value of the thermopower in Ni(Ti,Hf)Sn alloys as well as for NiTiSn compound reported in Ref. 19. However, this conclusion has still to be checked, since the Hall concentration has not been reported for these alloys. Moreover, the theoretical results give also some insights into the thermopower measurements,[10] which also inspired this work. These authors[10] reported very high ZT value based on a large value of the thermopower. Following the above-mentioned discussion (Sec. III) the variations of the thermopower presented in Fig. 2 of Ref. 10 could be attributed to variations of the carrier concentration.

[1] J. Pierre, R. Skolozdra, J. Tobola, S. Kaprzyk, C. Hordequin, M. A. Kouacou, I. Karla, R. Currat, and E. Lelievre-Berna, J. Alloys Compd. **262 & 263**, 101 (1997).
[2] R. A. de Groot, F. M. Mueller, P. G. van Engen, and K. H. J. Buschow, Phys. Rev. Lett. **50**, 2024 (1983).
[3] T. J. Zhu, L. Lu, M. O. Lai, and J. Ding, Smart Mater. Struct. **14**, S293 (2005).
[4] F. G. Aliev, F. G. Brandt, V. Moshchalkov, R. V. Skolozdra, and A. I. Belogorov, Z. Phys. B: Condens. Matter **75**, 167 (1989).
[5] J. Tobola, J. Pierre, S. Kaprzyk, R. Skolozdra, and M. A. Kouacou, J. Phys.: Condens. Matter **10**, 1013 (1998).
[6] C. Uher, J. Yang, S. Hu, D. T. Morelli, and G. P. Meisner, Phys. Rev. B **59**, 8615 (1999).
[7] S. J. Poon, Semicond. Semimetals **70**, 37 (2001).
[8] G. D. Mahan, *Good Thermoelectrics, Solid State Physics*, edited by H. Ehrenreich and F. Saepen, Vol. 51 (Academic Press, San Diego, 1998).
[9] H. Hohl, A. P. Ramirez, C. Goldmann, G. Ernst, B. Wolfing, and E. Bucher, J. Phys.: Condens. Matter **11**, 1697 (1999).
[10] S. Sakurada and N. Shutoh, Appl. Phys. Lett. **86**, 082105 (2005).
[11] S. Öğüt and K. Rabe, Phys. Rev. B **51**, 10443 (1995).
[12] P. Larson, S. D. Mahanti, and M. G. Kanatzidis, Phys. Rev. B **62**, 12754 (2000).
[13] P. Blaha, K. Schwarz, G. K. H. Madsen, D. Kvasnicka, and J. Luitz, *WIEN2K: An Augmented Plane Wave + Local Orbitals Program for Calculating Crystal Properties* (Karlheinz Schwarz, Techn. Universität Wien, Austria, 2001), ISBN 3-9501031-1-2.
[14] J. P. Perdew, K. Burke, and M. Ernzerhof, Phys. Rev. Lett. **77**, 3865 (1996).
[15] J. Tobola, J. Pierre, S. Kaprzyk, R. Skolozdra, and M. A. Kouacou, J. Magn. Magn. Mater. **159**, 192 (1996).
[16] J. Tobola, L. Jodin, P. Pecheur, H. Scherrer, G. Venturini, B. Malaman, and S. Kaprzyk, Phys. Rev. B **64**, 155103 (2001).
[17] S. Kaprzyk and A. Bansil, Phys. Rev. B **42**, 7358 (1990).
[18] A. Bansil, S. Kaprzyk, P. E. Mijnarends, and J. Tobola, Phys. Rev. B **60**, 13396 (1999).
[19] B. A. Cook, J. L. Harringa, Z. S. Tan, and W. A. Jesser, *15th International Conference on Thermoelectrics* (IEEE, Pasadena, CA, 1996).
[20] T. Katayama, S. W. Kim, Y. Kimura, and Y. Mishima, J. Electron. Mater. **32**, 1160 (2003).
[21] E. Arushanov, W. Kaefer, K. Fess, C. Kloc, K. Friemelt, and E. Bucher, Phys. Status Solidi A **177**, 511 (2000).
[22] L. Chaput, P. Pécheur, J. Tobola, and H. Scherrer, Phys. Rev. B **72**, 085126 (2005).